Modern Environmental Science and Engineering (ISSN 2333-2581)
August 2022, Volume 8, No. 8, pp. 405-414
Doi: 10.15341/mese(2333-2581)/08.08.2022/001
Academic Star Publishing Company, 2022
www.academicstar.us

Large Displacement Analysis With Material Nonlinear of Shell Structure Using New Flat Shell Elements

Anna Vardanyan[1], Norio Takeuchi[1], and Kenjiro Terada[2]

1. Hosei University, Japan

2. Tohoku University, Japan

Abstract: In this study, we propose a numerical algorithm for a nonlinear large displacement analysis method using flat shell elements in the hybrid-type penalty method (HPM). First, we describe the flat plate elements of HPM using the local coordinate system. Even with a flat plate, the adjacent elements have an angle at which a large displacement occurs. Next, we propose the relative displacement in this case. The "step-by-step method" is used as the algorithm for material nonlinear analysis and large displacement analysis. Finally, the accuracy of the solution of the proposed method is verified using a simple numerical example.

Key words: flat shell element, hybrid-type penalty method, large displacement, hinge

1. Introduction

The simulation of a series of phenomena in which fracture progresses from an elastic state, forms a collapse mechanism, and then moves discretely is called multi-stage fracture simulation (MSFS) [1]. In brittle materials, large displacement states (mainly rigid body displacements) often occur under the load state that forms the collapse mechanism. Therefore, in MSFS, a large displacement analysis is required as the numerical method.

For thin plate fracture analysis, such as glass plate fracture, it is convenient to use a plate or flat shell. However, a flat plate initially represented by a flat surface will have a curved surface when it is in a large displacement state. Therefore, in MSFS, the use of plate elements is not appropriate, and it is necessary to use flat shell elements.

In addition, the model order reduction (MOR) method [2] has attracted attention in the field of stress analysis, as it improves the efficiency of processing calculations by reducing the number of dimensions of the model. For example, numerical results can be obtained quickly by simplifying the computation process with low-dimensional elements such as flat shell elements. Flat shell elements can also be conveniently used to analyze other problems in sheet conditions, such as the stress analysis of sheet glass.

The development of shell elements for use in the finite element method has been underway since the 1960s [3], and new elements are still being researched. For example, Hamadi et al. [4] developed a flat shell element with four vertices in a quadrangle and one node within the element. In addition, benchmark problems were analyzed using general-purpose software. Burand and Angalekar [5] analyzed the benchmark nonlinear problem using ANSYS software. Lamine et al. [6] analyzed the benchmark problem using ABAQUS and compared their results with experimental values.

Many studies have been conducted on shell structures for geometric nonlinear problems, and Rivera et al. [7] verified their accuracy using elements with eight parameters. Sze et al. [8] also analyzed

Corresponding author: Norio Takeuchi, Dr., Professor, research areas: computational engineering & science. E-mail: takeuchi@hosei.ac.jp.

benchmark problems for various methods in geometric nonlinear problems.

In relation to the MOR mentioned earlier, a method using an interface element for the deformed connection has been proposed [9]. In recent years, models used in isogeometric analysis [10] have been developed [11, 12], and methods, such as the isogeometric inverse finite element method, have also been studied [13].

Generally, to evaluate the safety of a structure, it is necessary to understand its destruction state and collapse load. To solve these problems, the HPM was proposed [14-16]. In the HPM, an independent displacement field is assumed for each element. This displacement field is composed of rigid body displacement, strain, and gradient. HPM is suitable for the analysis of large displacement problems in which rigid body displacement is dominant.

The continuity of the displacement between the elements is approximated using a penalty function. Furthermore, the surface force is obtained from the relative displacement along the boundary between adjacent elements. By applying the fracture condition to the penalty function on the element boundary using this surface force, it is possible to introduce fracture phenomena, such as slip, crack, and hinge.

However, when flat shell elements are used to model the shell structure of a shape, the adjacent elements are joined diagonally; therefore, it is difficult to obtain the relative displacement between the different coordinate systems.

The purpose of this study is to develop a shell model that utilizes the advantages of HPM and an algorithm for material nonlinear large displacement analysis using the shell model. First, the displacement field represented by the local coordinate system, which is different for each element, is converted into the local coordinate system of one of the adjacent elements. Furthermore, it is converted into the coordinate system of the element boundary edge. We propose a method to calculate the relative displacement from the displacement of the boundary edge of the adjacent elements obtained in this manner.

2. Brief Formulation of Flat Shell Element

2.1 Formulation of Flat Shell Element [17]

In the HPM, the discretization equation is derived based on the hybrid virtual work equation:

$$\sum_{e=1}^{M} \delta W^{(e)} + \sum_{s=1}^{N} H_{<s>} = 0 \tag{1}$$

where M is the number of elements, N is the number of element boundary edges, (e) represents the e element $\Omega^{(e)}$, and <ab> represents the common boundary $\Gamma_{<ab>} := \partial\Omega^{(a)} \cap \partial\Omega^{(b)}$ of adjacent elements.

The first term represents the virtual work formula and the second term represents the formula for subsidiary conditions, as shown below:

$$\delta W^{(e)} = \int_{\Omega^{(e)}} \boldsymbol{\sigma} : \mathrm{grad}\delta\boldsymbol{u}\, dV - \int_{\Omega^{(e)}} \boldsymbol{f}\cdot\delta\boldsymbol{u} dV - \int_{\Gamma^{(e)}} \boldsymbol{t}\cdot\delta\boldsymbol{u}\, dS \tag{2}$$

$$H_{<s>} = -\delta \int_{\Gamma_{<s>}} \boldsymbol{\lambda}\cdot(\boldsymbol{u}^{(a)}_{<ab>} - \boldsymbol{u}^{(b)}_{<ab>})\, dS \tag{3}$$

where σ is stress, f is physical strength, u is displacement, δu is virtual displacement, and λ is the Lagrange multiplier.

Fig. 1 shows the degrees of freedom of the flat shell elements of the HPM. The proposed displacement field is expressed in Equations (4)-(6). The red letters represent the rigid-body displacement shown in Fig. 1.

$$u = u_0 - y\theta_z + x\varepsilon_x + \frac{1}{2}y\gamma_{xy} \tag{4}$$

$$v = v_0 + x\theta_z + y\varepsilon_y + \frac{1}{2}x\gamma_{xy} \tag{5}$$

$$w = w_0 + y\theta_x - x\theta_y - \frac{1}{2}x^2\varepsilon_{x,z} - \frac{1}{2}y^2\varepsilon_{y,z} - \frac{1}{2}xy\gamma_{xy,z} \tag{6}$$

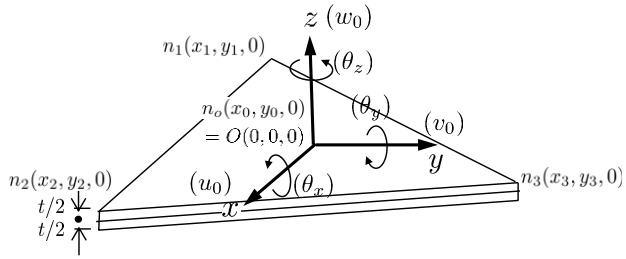

Fig. 1 DOF of flat shell element.

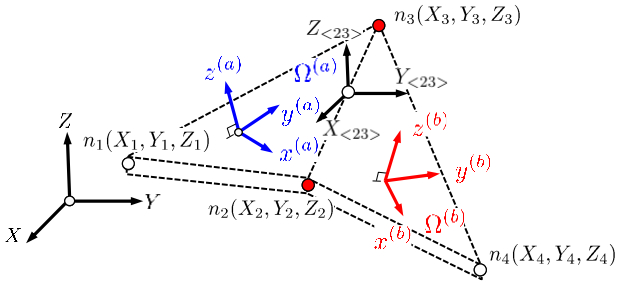

Fig. 2 Local coordinate system for each subdomain.

As shown in Fig. 2, $\boldsymbol{x}$ is a value in the local coordinate system *x*-*y*-*z* for each element and $\boldsymbol{X}$ is a value in the global coordinate system *X*-*Y*-*Z*. $\boldsymbol{R}_x$ is a coordinate transformation matrix between the global and local coordinate systems. The following relationship exists between the two:

$$\boldsymbol{x} = \boldsymbol{R}_x \boldsymbol{X} \tag{7}$$

Using these relationships, the following relationships exist between the local coordinate systems of adjacent elements.

$$\boldsymbol{x}^{(a)}_{<23>} = \boldsymbol{R}^{(a)}_x \left(\boldsymbol{R}^{(b)}_x\right)^{-1} \boldsymbol{x}^{(b)}_{<23>} \tag{8}$$

where, (*a*) and (*b*) represent the adjacent elements $\Omega^{(a)}$ and $\Omega^{(b)}$, respectively, and <23> represents the boundary edge n_2-n_3 as shown in Fig. 2.

The displacement field shown in Equations (4)-(6) is written as follows:

$$\boldsymbol{u}^{(e)} = \boldsymbol{N}^{(e)} \boldsymbol{U}^{(e)} \tag{9}$$

where, $\boldsymbol{u}^{(e)}$ is the displacement at an arbitrary point in element *e*, $\boldsymbol{U}^{(e)}$ is the degree of freedom of element *e*, and $\boldsymbol{N}^{(e)}$ is the coefficient matrix linking these. Displacement $\boldsymbol{u}^{(e)}_{<s>}$ at the boundary edge <s> of element (e) is defined as follows:

$$\boldsymbol{u}^{(e)}_{<s>} \overset{\text{def.}}{=} \boldsymbol{u}^{(e)}\Big|_{\Gamma_{<s>}} \tag{10}$$

The displacement $\boldsymbol{u}^{(e)}_{<s>}$ is represented by a local coordinate system provided for each element, and the displacement $\boldsymbol{u}^{(e)}_{n_{<s>}}$ converted into the coordinate system of the boundary edge of the element (e) is as follows:

$$\boldsymbol{u}^{(e)}_{n_{<s>}} = \boldsymbol{R}^{(e)}_{<s>} \boldsymbol{u}^{(e)}_{<s>} \tag{11}$$

where $\boldsymbol{R}^{(e)}_{<s>}$ is the matrix that transforms the local coordinate system of $\Omega^{(e)}$ into the coordinate system along element boundary <s>.

The displacement on the boundary side of the adjacent elements based on the local coordinate system of $\Omega^{(a)}$ is expressed as follows:

$$\boldsymbol{u}^{(a|a)}_{n_{<ab>}} = \boldsymbol{R}^{(a)}_{<ab>} \boldsymbol{u}^{(a)}_{<ab>} \tag{12}$$

$$\boldsymbol{u}^{(b|a)}_{n_{<ab>}} = \boldsymbol{R}^{(a)}_{<ab>} \boldsymbol{R}^{(a)}_x \left(\boldsymbol{R}^{(b)}_x\right)^{-1} \boldsymbol{u}^{(b)}_{<ab>} \tag{13}$$

where (b|a) is the displacement field of $\Omega^{(b)}$ represented by the local coordinate system of $\Omega^{(a)}$. The relative displacement $\boldsymbol{\delta}^{(a)}_{<ab>}$ with respect to the $\Omega^{(a)}$ coordinate system is obtained as follows:

$$\boldsymbol{\delta}^{(a)}_{<ab>} = \boldsymbol{u}^{(a|a)}_{n_{<ab>}} - \boldsymbol{u}^{(b|a)}_{n_{<ab>}} \tag{14}$$

By introducing the above displacement field relation into Equation (1), the discretization equation in the HPM based on the Kirchhoff theory can be obtained as follows:

$$\boldsymbol{K}_s \boldsymbol{U} = \boldsymbol{P}_s \tag{15}$$

$$\boldsymbol{K}_s = \sum_{e=1}^{M} \boldsymbol{K}^{(e)}_s + \sum_{s=1}^{N} \boldsymbol{K}_{s_{<s>}}, \quad \boldsymbol{P}_s = \sum_{e=1}^{M} \boldsymbol{P}^{(e)}_s,$$

where, $\boldsymbol{K}^{(e)}_s$ is the coefficient matrix obtained from the virtual work Equation (2), $\boldsymbol{K}_{s_{<s>}}$ is a coefficient matrix obtained from the incidental condition in Equation (3), and $\boldsymbol{P}^{(e)}_s$ is the load term for each element.

2.2 Accuracy of Elastic Solution

For the first example, we considered a semicircular curved beam with a pin support at one end and a roller support at the other end, as shown in Fig. 3(a). The shape of the semicircular curved beam was R = 0.16 m, d = 0.1 m, and t = 0.002 m. Young's modulus was E = 190 GN/m^2 and Poisson's ratio was 0. Geometrical moment of inertia was $I = 6.666 \times 10^{-11}$ m^4. A line load was applied at the top middle of the model: p = 1 kN/m $(P = p \times d = 100\ \text{N})$.

The theoretical result of the vertical displacement was

$$w_{\text{Theory}} = \frac{PR^3}{4EI}\left(\frac{3\pi}{2} - 4\right) = 5.759 \text{ mm}.$$

In addition, the vertical displacement of the frame model with 20 elements, as shown in Fig. 3(b), was computed as ω_f = 5.768 mm*wf*.

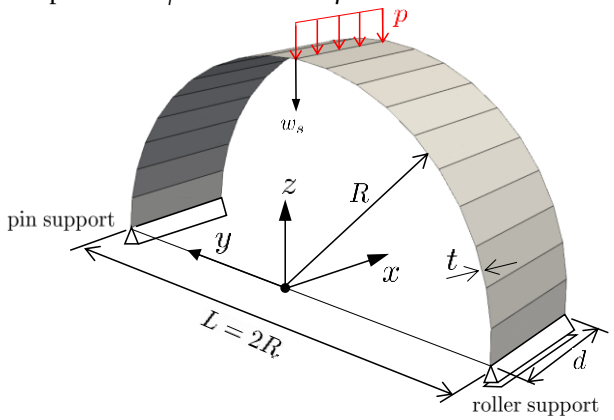

(a) Flat shell model

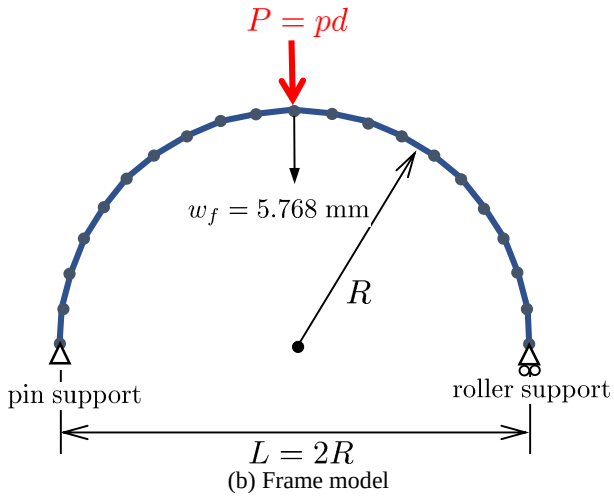

(b) Frame model

Fig. 3 Numerical model for accuracy of elastic solution.

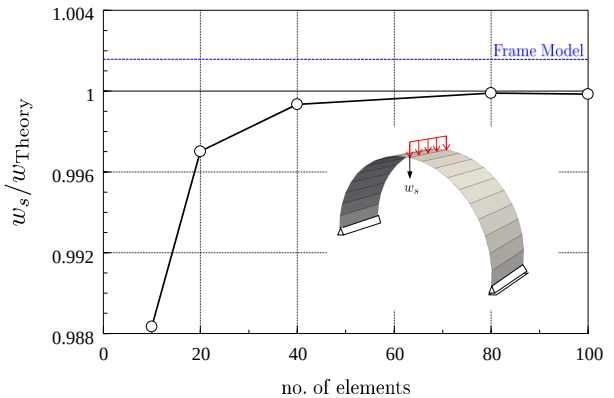

Fig. 4 Convergence of displacement solution by number of elements.

Fig. 4 shows the convergence of the displacement according to the number of elements. The circles represent the results of the flat shell model, and the blue line represents the results of the frame model with 20 elements. Fig. 5 shows the displacement distribution in the vertical direction.

2.3 Pinched Cylinder Analysis

For the second example, we considered a pinched cylinder with both ends free, as shown in Fig. 6. The shape of the cylinder was *L* = 0.9 m, *R* = 0.16 m, and *t* = 0.002 m. T Young's modulus was *E* = 190 GPa and Poisson's ratio was ν = 0.265. A point load *F* = 8.386 kN was applied at the top middle of the model.

Fig. 7 shows the convergence state of the vertical displacement of the loading point. The vertical axis represents the vertical displacement divided by the analytical solution.

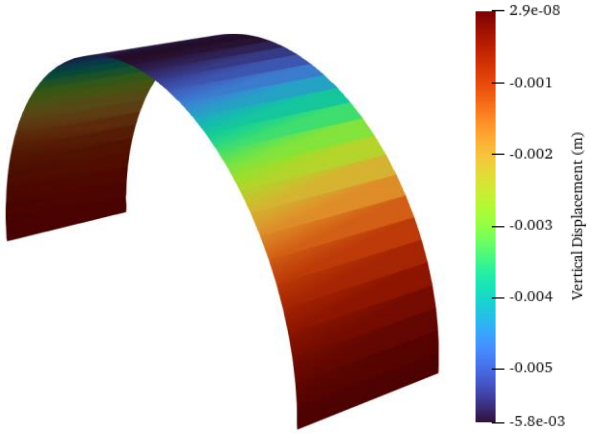

Fig. 5 Distribution for vertical displacements.

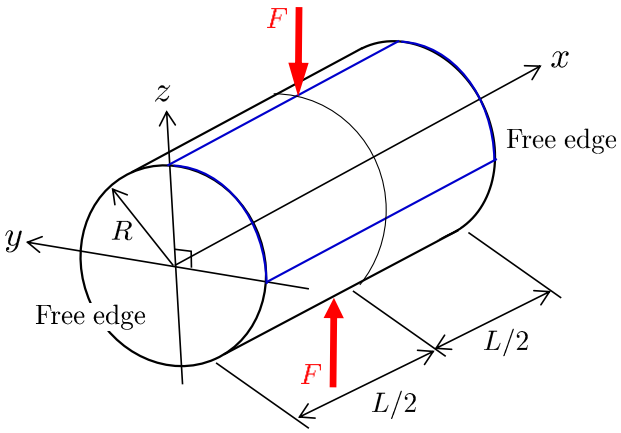

Fig. 6 Pinched cylinder with free edges.

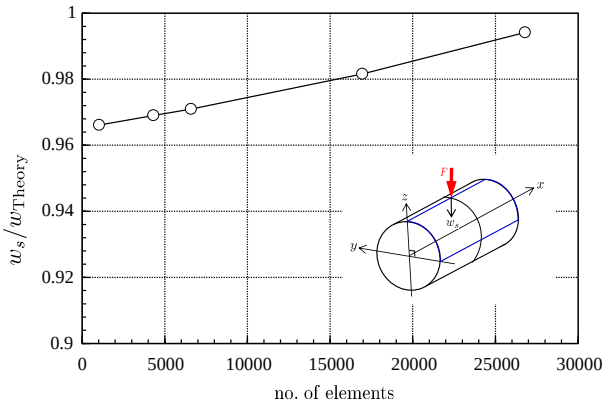

Fig. 7 Vertical displacement of loading point.

3. Material Nonlinear Analysis

3.1 Constitutive Equation for Surface Force

Discrete analysis using the HPM deals with two fractures: one within the element and the other between adjacent elements. In this study, we dealt only with failure at the edge between adjacent elements. In shell problems, fractures such as bending fractures, slip failures, and tensile cracking occur at the edges. We analyzed the progress of a hinge with a bending fracture.

Generally, the yield function $f(M,\sigma)$ and plastic potential $\Phi(M,\sigma)$ are

$$f(M,\sigma) = 0 \tag{16}$$

$$\Phi(M,\sigma) = 0 \tag{17}$$

Here, we assumed $f = \Phi$, according to the associated flow rule. A plastic hinge was assumed as the fracture condition of the flat shell model in the HPM. The fracture conditions in this case were as follows:

$$f(\boldsymbol{M}) = \frac{|M|}{M_y} - 1 \tag{18}$$

where M_y represents the full plastic moment.

We considered the increase in strain on the plastic hinge using the flow theory of plasticity. In this case, the incremental bending moment was obtained as follows:

$$\Delta M_n = k^{(p)} \Delta\delta \tag{19}$$

where Δδ represents the relative displacement, and the penalty function was defined as

$$k_{ij}^{(p)} = k_i^{(e)}\delta_{ij} - \frac{1}{\sum k_i^{(e)} f_i^2} f_i f_j k_i^{(e)} k_j^{(e)} \tag{20}$$

3.2 Load Incremental Method

For the nonlinear analysis, the “R mini method” [14] in the load increment method shown in Fig. 8 was used. The method first searches the boundary of the element for the smallest rate of load increment. At the element boundary where the hinge occurs, the coefficient matrix from Equation (15) is obtained using the incremental relationship of Equation (19), and the minimum rate of load increment is determined again. This process was repeated until all loads were applied.

It was assumed that the stress state would shift from point P to point R owing to the loading. Because the stress state cannot exceed the yield surface, it is necessary to return to point *Q*. The load whose stress state did not exceed the yield surface was obtained by multiplying the stress at point *R* by the increment rate, calculated as follows:

$$r = \frac{\overline{PQ}}{\overline{PR}} \tag{21}$$

Accordingly, the (i + 1)th acting load $\boldsymbol{P}^{(i+1)}$ can be obtained from the ith load $\boldsymbol{P}^{(i)}$ as follows:

$$\boldsymbol{P}^{(i+1)} = (1 - r_i)\boldsymbol{P}^{(i)} \tag{22}$$

The term r_i denotes the rate of load increment, which can be obtained from Equation (18) as follows:

$$f(\boldsymbol{M} + r \cdot \Delta\boldsymbol{M}) \le 0 \tag{23}$$

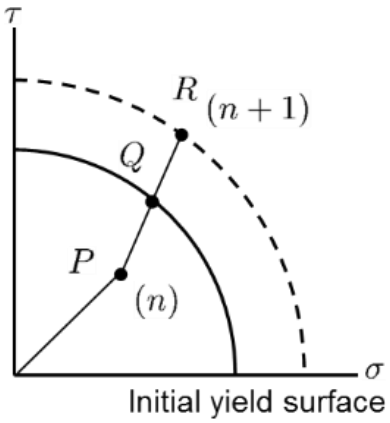

Fig. 8 Relationship between yield surface and stress state.

When the yield function is given by (18), the rate of the load increment is computed as follows:

$$\left(\frac{M_n + r \cdot \Delta M_n}{M_y}\right) - 1 = 0 \tag{24}$$

We obtained *r* as follows:

$$r = \frac{M_y + M_n}{\Delta M_n} \tag{25}$$

Therefore, the bending moment M^{n+1} after rearranging is:

$$\boldsymbol{M}^{n+1} = \boldsymbol{M}^n + r \cdot \Delta \boldsymbol{M} \tag{26}$$

In the case of bending moment, the residual load at the *n*th step will be

$$\boldsymbol{P}^{(n)} = \prod_{i=0}^{n-1} [(1 - r_i)] \, \Delta \boldsymbol{P} \tag{27}$$

The cumulative rate of load increment is as follows:

$$r_{TOTAL} = \sum_{k=1}^{n} \left(\prod_{i=0}^{k-1} [(1 - r_i)] \right) r_k \tag{28}$$

When r_{Total} = 1, an iteration is finished.

4. Large Displacement Analysis

4.1 Numerical Algorithm by Step-by-Step Method

A large displacement analysis is difficult to handle as a linear analysis, such as a small deformation analysis, because the stiffness matrix changes with the deformation of the object. In this study we used the step-by-step method to analyze the large displacement problem by repeating the small deformation analysis (see Fig. 9).

As shown in Fig. 9, the load acting on the object was divided into several incremental loads, and the small deformation problem was analyzed for each. The obtained displacement Δu^{n+1} was added to coordinate value x^n before deformation; the coordinate value was updated, and the shape after deformation was created as x^{n+1}. The previous stress was added to the incremental stress to obtain the total stress, a rigidity matrix was created with the new node coordinate values, and the linear analysis was repeated.

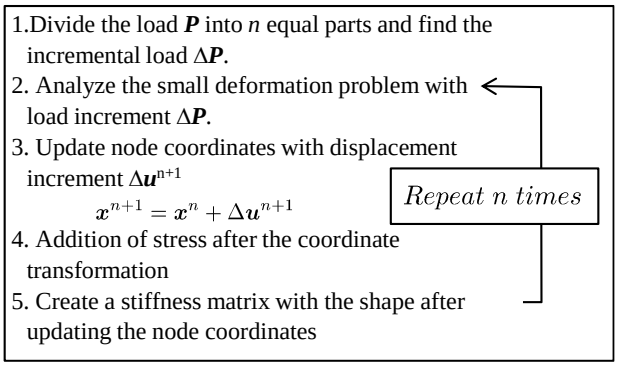

Fig. 9 Large displacement analysis method by step-by-step method.

4.2 Numerical Algorithm of Material Nonlinear Large Displacement Analysis

Fig. 10 shows the analysis flow of the large displacement problem with material nonlinearity proposed in this study. As shown in the figure, the solution was first obtained by linear analysis of the small deformation problem.

Next, the load increment rate for the material nonlinear problem was obtained, and the load increment rate owing to the limit rotation angle for the large deformation problem was obtained in (*1). This parameter was the limit value per increment set to prevent an increase in error due to the increase in the angle of rotation of the rigid body. The minimum load increment rate was calculated by (*2). For stress, a coordinate transformation was applied in (*3).

Subsequently, the cumulative load increment rate was computed using (*4). If this value was less than one, the coordinates were updated, and the linear analysis was repeated with the remaining load.

4.3 Numerical Example of Large Displacement Analysis

In this section, we verify the accuracy of the solution of the large displacement analysis using the proposed step-by-step method for the elastic problem of a flat shell. Fig. 11 shows the model and mesh divisions used in the analysis. As shown in the figure, the numerical model was a flat plate with one fixed end, and the dimensions were as shown in the figure.

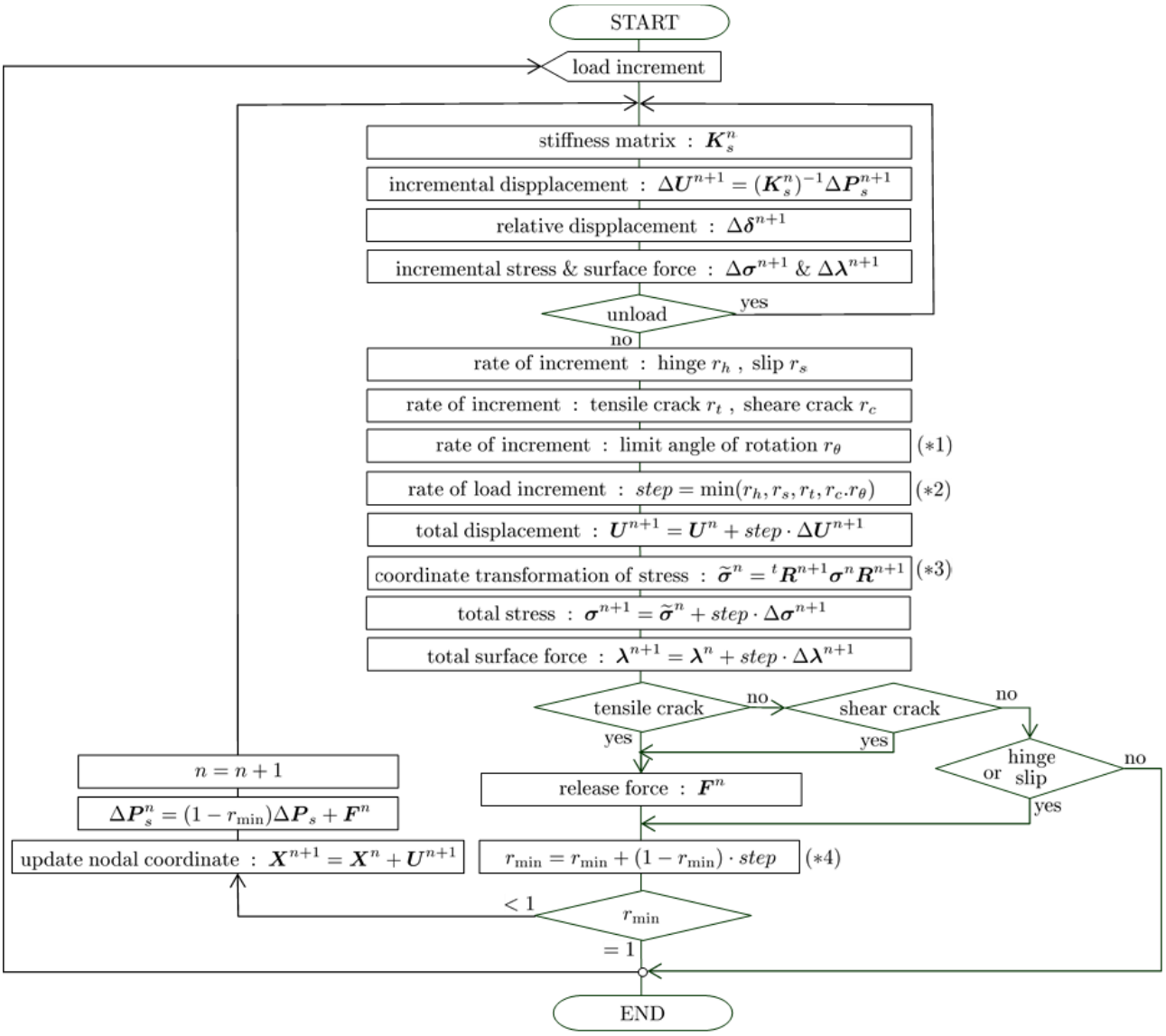

Fig. 10 Analysis flow of large displacement problem by step-by-step method with hinge condition.

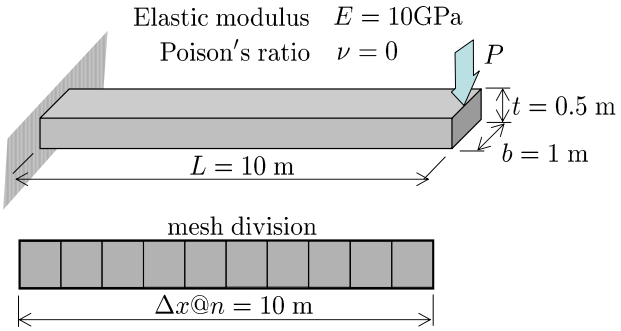

Fig. 11 Numerical model for cantilever.

The material constants used in this analysis are shown in the figure. The mesh was divided as shown in the lower part of the figure, but the number of divisions was analyzed assuming various cases.

In Fig. 12, the horizontal axis is the limit rotation angle and the vertical axis is the value obtained by dividing the deflection at the free end by the solution according to beam theory. The red circle represents the deflection at the free end and the blue triangle represents the horizontal displacement. A convergent solution was obtained when the limit rotation angle was set to 0.05 or less. Expressed in degrees, this is approximately 2.860 because $\sin(2.860) \approx 0.0499$.

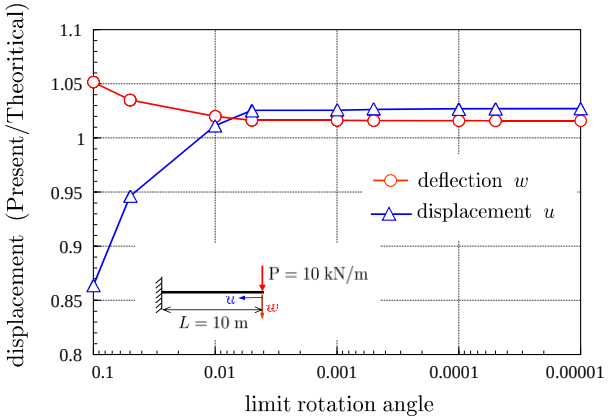

Fig. 12 Accuracy of displacement and deflection with different limit rotation angles.

Fig. 13 shows the dimensionless deflection of the free end of the flat plate on the horizontal axis and the dimensionless load on the vertical axis. Horizontal displacement does not occur in infinitesimal deformation problems. The red and black solid lines show the large displacement solution according to beam theory, and the solution based on infinitesimal deformation theory, respectively. The blue circles represent the solutions obtained using the proposed method: the results are very similar.

In contrast, in Fig. 14 the horizontal axis shows the dimensionless horizontal displacement value and the vertical axis shows the dimensionless load. The solid red line and the blue circles represent the large displacement solutions based on beam theory and the solutions obtained using this method, respectively: the results are very similar.

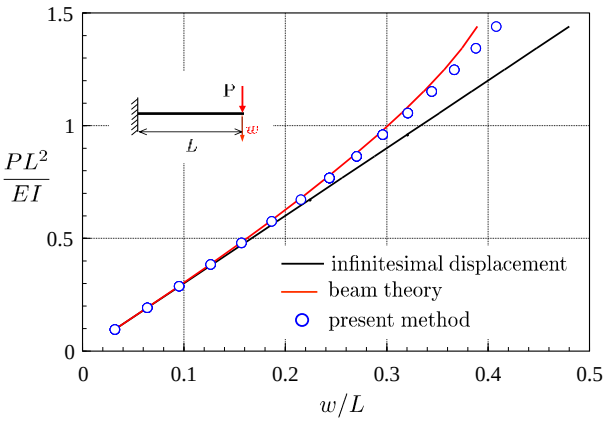

Fig. 13 Relationship between Load and Large Deflection.

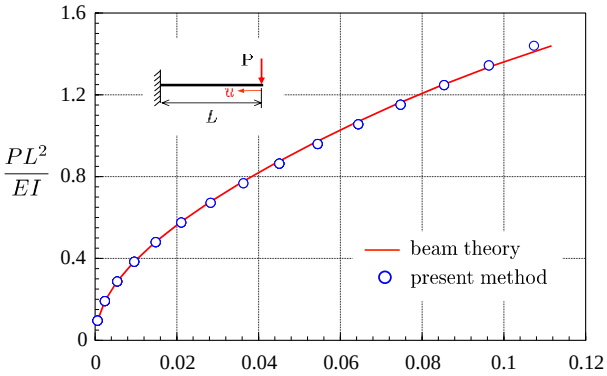

Fig. 14 Relationship between load and lateral displacement.

Fig. 15 shows the displacement mode. The figure shows an example of 20 divisions, and the deflection and horizontal displacement are shown to scale.

4.4 Numerical Example of Large Displacement Analysis with Hinge

Fig. 16 shows the model and mesh divisions used in the analysis. As shown in the figure, the numerical model was a portal frame with both ends fixed, and the dimensions were as indicated in the figure.

In the nonlinear analysis, we assumed that only the plastic hinge was generated and only the total plastic moment was set. The material constants used in this analysis are shown in the figure. As shown on the right side of the figure, the mesh was divided into 50 rectangular elements for each column and beam member, for a total of 150.

Fig. 17 shows the dimensionless displacement of the upper-right corner of the frame on the horizontal axis and the dimensionless load on the vertical axis. The solid red and black lines show the results of the proposed large displacement analysis and the infinitesimal deformation by beam theory, respectively. The dashed blue line indicates the limit load according to beam theory. The collapse load owing to infinitesimal deformation was consistent with the solution of the limit analysis; and the collapse load of the large displacement solution was slightly higher.

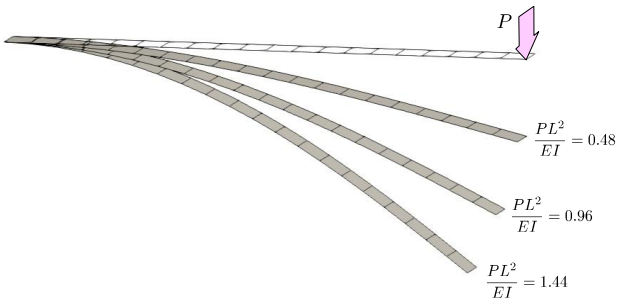

Fig. 15 Displacement mode per load.

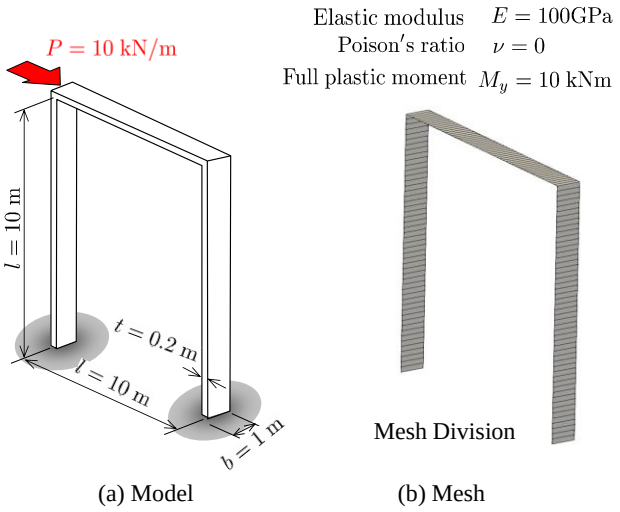

Fig. 16 Numerical model for gate frame.

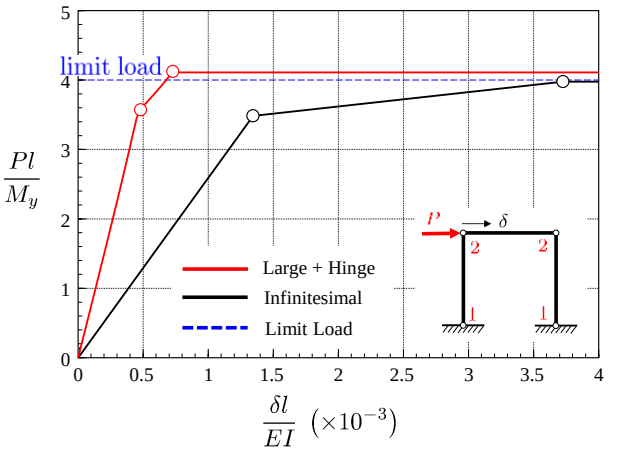

Fig. 17 Load displacement curve for large displacement analysis with hinge condition.

Fig. 18 shows the diagram of the displacement mode under a collapse load.

5. Conclusion

In this paper, we proposed a numerical method for the material nonlinear large displacement problem

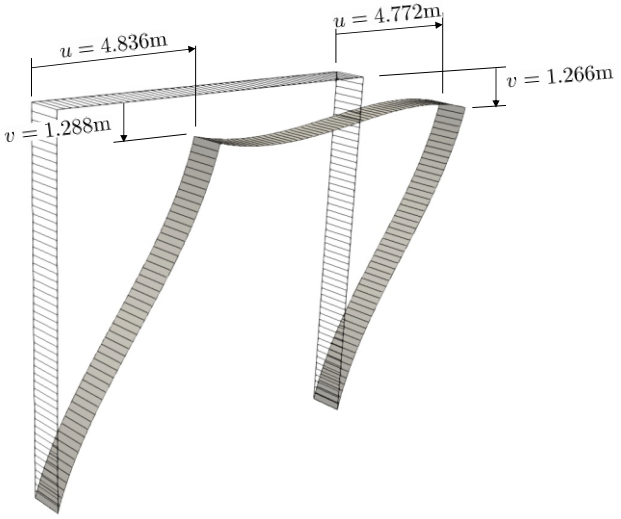

Fig. 18 Displacement mode at collapse load for portal frame fixed at both ends.

using flat shell elements in the HPM. As the HPM uses an independent displacement field for each element, the displacement field can be expressed using the local coordinate system set for each element. The application of this displacement field is appropriate for shell elements based on the Kirchhoff-Love theory, which superimposes in-plane and out-of-plane deformations.

However, in the HPM, which introduces continuity of displacement using a penalty function, it is difficult to handle the relative displacement in the case of a shell structure in which adjacent elements are not flatly connected. In this study, we proposed a method to transform the displacement into one of the local coordinate systems of adjacent elements in the calculation of the relative displacement. The effectiveness of this method was confirmed using a simple numerical example.

Next, the algorithm for material nonlinear analysis was shown. Because the HPM requires a surface force at the element boundary, it is easy to introduce slips, cracks, and hinges between elements. In this study, we proposed a method for introducing a hinge using the bending moment at the element boundary. When the infinitesimal deformation problem was analyzed using the proposed method, a collapse load consistent with the limit analysis solution was obtained.

We proposed an algorithm that can be applied to large displacement problems. From a simple numerical analysis, it was clarified that the solution obtained by this method yields the same result as the large displacement solution obtained by beam theory.

Finally, we proposed an algorithm for material nonlinear large displacement analysis that combines the algorithm of large displacement analysis and material nonlinear analysis. We were able to demonstrate the characteristics of the solution obtained by the proposed method using a simple numerical example.

References

[1] K. Yamaguchi, K. Yamamura, N. Takeuchi and K. Terada, Multi-stage fracture simulation of framed structure using HPM, *Journal of Japan Society of Civil Engineers A2*, 75 (2019) (2) I_225-I_236.

[2] Z. Q. Qu, Model Order Reduction Techniques with Applications in Finite Element Analysis, Springer-Verlag, 2004.

[3] S. Ahmad, B. M. Irons and O. C. Zienkiewicz, Analysis of thick and thin shell structures by curved finite elements, *Int. Journal for Numerical Methods in Engineering* 2 (1970) 419-451.

[4] D. Hamadi, A. Ayoub and O. Abdelhafid, A new flat shell finite element for the linear analysis of thin shell structures, *European Journal of Computational Mechanics* 24 (2016) (6) 232-255.

[5] J. Burand and S. S. Angalekar, Non-linear finite element analysis of shells using parametric study, *International Journal of Engineering Science & Research Technology* 6 (2017) (7) 116-121.

[6] D. M. Lamine, D. Hamadi, O. Temami, A. Ashraf and K. Abdelhak, Effect of boundary conditions and geometry on the failure of cylindrical shell structures, *Engineering Solid Mechanics* 8 (2020) 313-322.

[7] M. G. Rivera, J. N. Reddy and M. Amabili, A continuum eight-parameter shell finite element for large deformation analysis, *Mechanics of Advanced Materials and Structures* 27 (2020) (7) 551-560.

[8] K. Y. Sze, X. H. Liu and S. H. Lo, Popular benchmark problems for geometric nonlinear analysis of shell, *Finite Elements in Analysis and Design* 40 (2004) (11) 1551-1569.

[9] A. R. Silva and L. E. S. Dias, An interface element for numerical analysis of flat plate/shell elements with deformable connection, *Latin American Journal of Solid and Structures* 15 (2018) (2) 1-16.

[10] J. A. Cottrell, T. J. R. Hughes and Y. Bazileves, *Isogeometric Analysis*, John Wiley and Sons, 2009.

[11] J. Kiendl, K. U. Bletzinger, J. Linhard and R. Wuchner, Isogeometric shell analysis with Kirchhoff-Love element, *Computer Methods in Applied Mechanics and Engineering* 198 (2009) (49) 3902-3914.

[12] D. Schollhammer, B. Marussig and T. P. Fries, A consistent higher-order isogeometric shell formulation, *arXiv:2012.11975v1*, 1-51, 2020.

[13] A. Kefal and E. Oterkus, Isogeometric iFEM analysis of thin shell structures, *Sensors* 20 (2020) 1-24.

[14] N. Takeuchi, H. Ohki, A. Kambayashi and M. Kusabuka, Material non-linear analysis by using discrete model applied penalty method in hybrid displacement model, *Transactions of JSCES*, Paper no. 20010002, 53-62, 2001.

[15] A. Vardanyan and N. Takeuchi, Discrete analysis for plate bending problems by using hybrid-type penalty method, *Bulletin of Research Center for Computing and Multimedia Studies*: *Hosei University* 21 (2008) 131-141.

[16] N. Takeuchi and A. Vardanyan, Elasto-plastic analysis for plate bending problems by using hybrid-type penalty method, *Bulletin of Chuvash State Pedagogical University* 6 (2009) 179-194.

[17] A. Vardanyan and N. Takeuchi, Development of a flat shell element in hybrid-type penalty method, *Bulletin of Research Center for Computing and Multimedia Studies: Hosei University* 35 (2020) 21-35.